A&A 648, A88 (2021)
https://doi.org/10.1051/0004-6361/202140343

Astronomy & Astrophysics

In search of Bennu analogs: Hapke modeling of meteorite mixtures

F. Merlin[1], J. D. P. Deshapriya[1], S. Fornasier[1,2], M. A. Barucci[1], A. Praet[1], P. H. Hasselmann[1], B. E. Clark[3], V. E. Hamilton[4], A. A. Simon[5], D. C. Reuter[5], X.-D. Zou[6], J.-Y. Li[6], D. L. Schrader[7], and D. S. Lauretta[6]

[1] LESIA, Observatoire de Paris, Université PSL, CNRS, Université de Paris, Sorbonne Université, 92195 Principal Cedex Meudon, France
e-mail: frederic.merlin@obspm.fr
[2] Institut Universitaire de France (IUF), 1 rue Descartes, 75231 Paris CEDEX 05, France
[3] Department of Physics and Astronomy, Ithaca College, Ithaca, NY, USA
[4] Southwest Research Institute, Boulder, CO, USA
[5] NASA Goddard Space Flight Center, Greenbelt, MD, USA
[6] Lunar and Planetary Laboratory, University of Arizona, Tucson, AZ, USA
[7] Center for Meteorite Studies, School of Earth and Space Exploration, Arizona State University, AZ, USA

Received 14 January 2021 / Accepted 5 March 2021

ABSTRACT

Context. The OSIRIS-REx Visible and InfraRed Spectrometer onboard the Origins, Spectral Interpretation, Resource Identification, and Security-Regolith Explorer spacecraft obtained many spectra from the surface of the near-Earth asteroid (101955) Bennu, enabling the characterization of this primitive small body. Bennu is spectrally similar to the hydrated carbonaceous chondrites (CCs), but questions remain as to which CCs, or combinations thereof, offer the best analogy to its surface.
Aims. We aim to understand in more detail the composition and particle size of Bennu's surface by refining the relationship between this asteroid and various CC meteorites.
Methods. We used published absorbance and reflectance data to identify new optical constants for various CC meteorites measured in the laboratory at different temperatures. We then used the Hapke model to randomly generate 1000 synthetic spectra in order to find the combinations of these potential meteoritic analogs that best reproduce the spectral features of the asteroid.
Results. Our investigations suggest that the surface of Bennu, though visibly dominated by boulders and coarse rubble, is covered by small particles (tens to a few hundreds of μm) and that possibly dust or powder covers the larger rocks. We further find that the surface is best modeled using a mixture of heated CM, C2-ungrouped, and, to some extent, CI materials.
Conclusions. Bennu is best approximated spectrally by a combination of CC materials and may not fall into an existing CC group.

Key words. techniques: spectroscopic – minor planets, asteroids: individual: (101955) Bennu – methods: observational – methods: data analysis

1. Introduction

In early December 2018, NASA'S Origins, Spectral Interpretation, Resource Identification and Security-Regolith Explorer (OSIRIS-REx) spacecraft arrived at the near-Earth asteroid (101955) Bennu, with the objective to study the surface of this small primitive object and return a sample of pristine carbonaceous regolith to Earth (Lauretta et al. 2017, 2021). Bennu is spectrally classified as a B-type asteroid, part of the larger C-complex of asteroids, with visible to near-infrared spectral properties resembling those of carbonaceous chondrite meteorites, particularly the CMs and CIs (Clark et al. 2011; Hamilton et al. 2019; Simon et al. 2020). These meteorites are water- and organic-bearing and may have delivered such materials to Earth early in Solar System history.

Bennu is among the darkest objects of the Solar System, with a global mean normal albedo of about 4.4% (Lauretta et al. 2019). However, in contrast to the asteroid Ryugu, which exhibits a homogeneously dark surface (Kitazato et al. 2019), images acquired by the OSIRIS-REx Camera Suite (OCAMS) reveal an unexpected degree of albedo heterogeneity on Bennu, with a ratio of reflected to incident flux ranging roughly from 3 to 15% (Lauretta et al. 2019) and normal albedo mainly ranging from 1.5 to 17% (Golish et al. 2021). The differences in albedo generally correspond to two primary boulder populations that dominate Bennu's rubble-covered surface (DellaGiustina et al. 2019, 2020). Rocks on Bennu are broken down by processes such as thermal fatigue (Molaro et al. 2020) and meteoroid bombardment (Bottke et al. 2020; Ballouz et al. 2020).

Spectral investigation performed using the OSIRIS-REx Visible and InfraRed Spectrometer (OVIRS, Reuter et al. 2018) and Thermal Emission Spectrometer (OTES, Christensen et al. 2018) has revealed evidence of abundant hydrated phyllosilicates that are widespread on Bennu's surface (Hamilton et al. 2019). Bennu's spectrum in the [0.4–2.4] μm range appears featureless with a negative slope, confirming previous ground-based observations (Clark et al. 2011; Binzel et al. 2015). All OVIRS spectra exhibit a near-infrared absorption feature near 2.7 μm, and together with thermal infrared spectral features observed at longer wavelengths, the data confirm the spectral resemblance of Bennu to the aqueously altered CM-type carbonaceous chondrites (Hamilton et al. 2019). In a multivariate statistical analysis of OVIRS spectral data, Barucci et al. (2020) find a spectrally homogeneous surface, as seen in the near-infrared range. No significant multimodality or grouping has been found to depend on the band area or band depth, although small variations in

band area or depth at 2.74 μm have been observed (Simon et al. 2020).

In more recent works, Simon et al. (2020) focused their analyses on the spectral features in the 3.4 μm region. This feature is ubiquitous on the surface of Bennu at different spatial scales, with the deepest 3.4 μm absorptions occurring on individual boulders. This feature is distinct from that seen on other C-complex asteroids for which the attribution was for primarily aliphatic organic molecules or carbonates (for Themis-like asteroids or Ceres-like asteroids, respectively). In individual spot spectra of Bennu, the shape and depth of this absorption feature vary and are similar to those of Themis and Ceres, along with other main-belt asteroids, indicating potential compositional variation in the carbon-bearing materials.

Kaplan et al. (2020) investigate this 3.4 μm absorption feature more thoroughly using OVIRS spectra acquired from different locations surrounding Nightingale, the site from which the OSIRIS-REx spacecraft collected a sample in October 2020. They found good fits with laboratory spectra of calcite, dolomite, magnesite, and meteorite insoluble organic matter (IOM). They conclude that bright veins observed in boulders are probably filled by carbonate. Regions of the surface that are relatively rich in IOM probably have experienced little thermal alteration. Elevated temperatures and space weathering should quickly alter these absorption features, so the strongest organic spectral features are likely connected with the most recently exposed surfaces.

To further refine the understanding of the compositional and physical surface properties of Bennu, as observed by the OVIRS instrument, here, we present a new approach in which we applied the Hapke model to interpret Bennu spectra using carbonaceous chondrites as input. This model is able to generate synthetic spectra of various mixtures of materials, with the possibility to change the particle size of each constituent. Such spectral modeling could efficiently constrain the abundance and particle size of the constituents of any atmosphereless body and has been widely used (see Reddy et al. 2015, for a short review). Models of radiative transfer involve computing reflectivity based on optical constants and particles' sizes of specific mineral species. However, this model ultimately requires optical constants of the constituent materials, and the number of available optical constants is very limited. This lack usually restricts models to simple areal mixtures of different materials, consisting of a linear mixture of reflectance spectra, for which reflectance spectra have been obtained in the laboratory, or to simple spectral comparisons as done in previous works (see Kaplan et al. 2020, for instance). To solve this problem, in this work we used laboratory data to generate optical constants of carbonaceous chondrites that were not previously available. We then used the Hapke model to synthesize spectra of various mixtures of the meteorites and amorphous carbon and assessed which are the best matches to the global spectrum of Bennu.

2. OVIRS data acquired at Bennu

The OVIRS hyperspectral point spectrometer operates in the spectral range of 0.4–4.3 μm. It has a circular aperture with a field of view of 4 mrad (Reuter et al. 2018). The data were calibrated according to the procedure detailed in Simon et al. (2018). The calibrated data were converted to the reflectance factor (REFF) and photometrically corrected to the standard geometry of $i = 30°$, $e = 0°$, and $\alpha = 30°$ (Zou et al. 2020).

We derived an average global spectrum from different spectra (Reuter et al. 2019) acquired during the 2019 May 9 Equatorial Station 3 observation of the Detailed Survey mission phase (Lauretta et al. 2017, 2021), which covered ±50°latitude with a spatial resolution of 19 m. These data were obtained at similar phase angles ($7.8° < \alpha < 10.4°$), which provide high signal-to-noise ratios (S/Ns) and minimize the uncorrected effects of the phase slope and phase reddening (Fornasier et al. 2020). Each of the 778 spectra, which follow our criteria (i.e., acquired in the ±50°latitude range), was normalized at 2.2 μm to the mean reflectance value of the whole set of selected spectra. Variability at each wavelength was computed as the quadratic error composed of the standard deviation of the 778 normalized spectra and the mean individual error divided by $\sqrt{778}$.

3. Laboratory data and spectral modeling

To compare the spectra of Bennu with synthetic spectra generated using the Hapke model, we needed to retrieve several input parameters. Among these inputs, the optical constants are the most important to generate reflectance spectra of different mixtures of meteorites that may represent the properties of the surface of Bennu.

3.1. Generation of optical constants from absorbance measurements

To generate optical constants for possible meteorite analogs of Bennu, we used absorbance parameters of materials determined in the laboratory from which we could extract accurate optical constants using scripts based on the Kramers-Kroning method (Rocha & Pilling 2014). We used absorbance data available from the SHHADE data base[1], published in Beck et al. (2014) and reported in Table 1. Although Bennu most closely resembles CMs and to some extent CIs (Clark et al. 2011; Hamilton et al. 2019), we tested all carbonaceous chondrite materials for which the absorbance data are available – including some CV, CK, CR, and ungrouped meteorites – for a comprehensive analysis.

All materials listed in Table 1 have been analyzed at three different temperatures (ambient or 22°C, mildly heated at 150°C, and more severely heated at 300°C). Unfortunately, the data are limited to the [2–4] μm range (versus the OVIRS spectral range of 0.4–4.3 μm), but this spectral range allowed us to analyze the near-infrared continuum from 2 to 2.6 μm and the complete structure of the absorption bands located in the [2.6–3.4] μm range.

We used a script to generate the optical constants from these data, detailed in Rocha & Pilling (2014). In this method, we initialized the value of n_0 (initial value of the real part of the refractive index) to a reasonable 1.7, because this value is commonly seen for a range of materials (see Roush 2003, for estimated optical constants of the Tagish Lake meteorite). We note that n_0 was only initialized; the values of n over the entire wavelength range were then adjusted by the method (as well as the values of k, the imaginary part of the refractive index). We also made an assumption about the particle size of the material from which the absorbance values were computed. The meteorite powders, which were crushed and sieved in the [5–15] μm range, were embedded in a 8-mm-thick KBr matrix, so we can infer a particle size on the order of a few microns given that the mass ratio of the material in the matrix is ~1:300. For the purpose of our analysis, we adopted a slightly high estimated particle size of the 10 μm version, corresponding to the initial mean particle size of the meteorite powder. The sizes retrieved by our models therefore could be slightly overestimated.

[1] https://www.sshade.eu/search/spectrum

Table 1. Material used to generate new optical constants.

From absorbance data				
CI chondrite				
Ivuna *CI1*	Orgueil *CI1*			
CR chondrite				
GRA 06100 *CR2*	GRO 03116 *CR2*	GRO 95577 *CR1*	LAP 02342 *CR2*	
CM chondrite				
ALH 83100 *CM1/2*	ALH 84044 *CM2*	Boriskino *CM2*	DOM 08003 *CM2*	EET 96029 *CM2*
LEW 85311 *CM2-an*	LEW 87022 *CM2*	LON 94101 *CM2*	MCY 05230 *CM2*	MIL 07700 *CM2*
Murchison *CM2*	Niger *CM2*	Nogoya *CM2*	PCA 91008 *CM2-an*	QUE 99355 *CM2*
QUE 97990 *CM2*	WIS 91600 *CM-an*			
CV chondrite				
Grosnaja *CV3*	Kaba *CV3*	Mokoia *CV3*	Vigarano *CV3*	
C2-ungrouped chondrite				
Bells	Essebi			
CK chondrite				
ALH 85002 *CK4*	Maralinga *CK4-an*	EET 92002 *CK5*		
From reflectance data				
Alais *CI1*	Crescent *CM2*	EET 83226 *C2-ung*	Essebi *C2-ung*	Mokoia *CV3*
Murchison *CM2*	Orgueil *CI1*	Tagish Lake *C2-ung*		

Notes. ALH = Allan Hills, DOM = Dominion Range, EET = Elephant Moraine, GRA = Graves Nunatak, GRO = Grosvenor Range, LAP = LaPaz, LEW = Lewis Cliff, LON = Lonewolf Nunataks, MCY = MacKay Glacier, MET = Meteorite Hills, MIL = Miller Range, PCA = Pecora Escarpment, and WIS = Wisconsin Range.

3.2. Spectral modeling

We used the spectral model developed by Hapke (1981, 1993) to generate synthetic spectra. This model allowed us to determine the reflectance spectra or the albedo of a medium from individual physical properties of the different components (with optical constants). We first briefly present the basis of the Hapke model to investigate the surface properties of Bennu. All the developments of the model are presented in Hapke (1981, 1993). In our case, we neglected light interferences and approximated the reflectance of the surface as

$$\mathrm{REFF}(\mu_0, \mu, \alpha) = \frac{w}{4\pi}\frac{\mu_0}{\mu_0+\mu}[((1+B(\alpha))P(\alpha)+H(\mu_0)H(\mu)-1)], \quad (1)$$

where $\mathrm{REFF}(\mu_0, \mu, \alpha)$ is the reflectance computed for a given set of an incidence angle ($\mu_0 = \cos(i)$), emittance angle ($\mu = \cos(e)$), and phase angle α. We note that w is the single-scattering albedo and depends on the optical constants of the particles and is described in Hapke (1981); $B(\alpha)$ is the ratio of the near-surface contribution to the total particle scattering (Hapke 1986); and $P(\alpha)$ is the phase function, which depends on the phase angle. The phase function describes the angular distribution of light reflected from a body. Furthermore, $H(\mu_0)$ and $H(\mu)$ take into account the multiple scattering of light by surface particles and were computed as follows (with $j = \mu$ or μ_0):

$$H(j) = \frac{1+2j}{1+2j\sqrt{1-w}}. \quad (2)$$

We followed the formalism of Emery & Brown (2004) to compute w from different compounds, assuming a "salt and pepper" or "intimate" mixture. In this work, we assume that all the particles of the medium have a similar phase function and, for simplification, the resulting photometric parameter corresponding to $(1+B(g))P(g)-1$ is represented by one global free parameter only (i.e., only one photometric parameter was adjusted for a given synthetic spectrum). This is mainly motivated by the fact that most of the parameters cannot be disentangled (Takir et al. 2015). Hapke developed refinements of his model to correct for macroscopic surface roughness (Hapke 1984) and porosity (Hapke 2008). They are not taken into account due to the large number of parameters already included in the models and since we consider a normalized model in this work, in which w and H contain most of the spectral information.

3.3. Generation of optical constants from reflectance data

To increase the number of optical constants of possible analogs, we also used the Hapke model to extract optical constants from reflectance data. Indeed, the general formalism of Eq. (1) allowed us to link the bidirectional reflectance to the average single-scattering albedo (w) of a sample, which is itself linked to the optical constants (see Hapke 1981). From this formalism, it is possible to derive k from the bidirectional reflectance if n and the size of the materials are well constrained. For this purpose, we used the laboratory data reported by Takir et al. (2019) from which the size of the samples was constrained to [50–100] μm. We used the reflectance data acquired in asteroid-like conditions (vacuum and thermally desiccated), and we selected the best eight analogs (Table 1, bottom row) by direct comparison of the reflectance spectra in the near-infrared range. The n value is more difficult to establish in this case (i.e., without the Kramers-Kroning method), but the value of n does not vary more than the percent level from the visible to the near-infrared range for a wide variety of materials. So, we inferred a quasi-constant n

value (i.e., we expect a variation of 1% compared to the average value) in the wavelengths covered by the OVIRS instrument and set this value at 1.7 for the [2–3.8] μm range. Once n was fixed, we iterated the k value for each wavelength to compute w and numerically adjusted the synthetic reflectance value (REFF) to the measured one. The accuracy of the iteration step for k is always better than 0.1%.

The optical constants generated with this method should be used with a bit more caution. In addition to the problem explained with the choice of n, the use of reflectance spectra as inputs to extract n and k values is subject to B and P functions, which are both unknown. The Hapke model is assumed to take into account these parameters; however, without knowing complete phase functions of the samples, we expect some discrepancies using different values of incidence, emission, and phase angles. These discrepancies should be limited because the Bennu data have been corrected and scaled for the same observational geometry as those of the laboratory measurements (i.e., $i = 30°$, $e = 0°$, $\alpha = 30°$). The second limitation of the extraction of such optical constants is the fact that the size parameter is not accurate; samples have been ground into fine powders (50–100 micrometers), but the size distribution was not well characterized. Thus, the significance of the extracted size parameters is limited.

3.4. Limits of the models

To search for the best free parameters that fit the surface spectra of Bennu, we derived abundances and a particle size by means of Marquardt-Levenberg minimization (Marquardt 1963; Levenberg 1944). This algorithm allowed us to obtain a minimization of the reduced χ^2 between synthetic spectra and the reflectance spectra of Bennu. However, the results are not unique because similar reduced χ^2 values can exist with different parameter combinations. The use of more or less dark material can reduce or increase the albedo of the synthetic spectrum and compensate for the use of larger or smaller amounts of bright compounds. At the same time, different combinations could produce similar absorption features. For example, the same depths and widths of absorption bands could be obtained from a combination of small numbers of large particles or large numbers of small particles. However, we used different initial conditions to take the best result into account in terms of reduced χ^2. On the other hand, the reduced χ^2 is a mathematical result that can favor large-scale features (spectrum continuum for instance) rather than the small ones (absorption bands). Moreover, the S/N of our spectra reaches its peak in the [2–3] μm range, and the results are mainly constrained in this range because the standard deviation of the data is used in the algorithm to determine the best reduced χ^2. The calibration is least well-constrained in the [2.6–3] μm range, and the thermal tail removal procedure could also affect the fits roughly longward ~3.4 μm (Simon et al. 2020).

To understand how the initial choice of the n_0 parameter affects our method, we extracted the optical constants for the CM chondrite ALH 83100 at 150°C (we chose ALH 83100 for this test because it is one of the best candidates to fit the Bennu spectrum) considering various n_0 parameters (i.e., 1.3, 1.7, and 2.1). Once the optical constants were extracted for each n_0, we generated two synthetic reflectance spectra from the pure ALH 83100 sample, considering the higher case of n_0 at 2.1 and two different particle sizes (10 and 100 μm). We then used the Hapke model to fit these two initial synthetic spectra considering an intimate mixture of an ALH 83100 sample with amorphous carbon

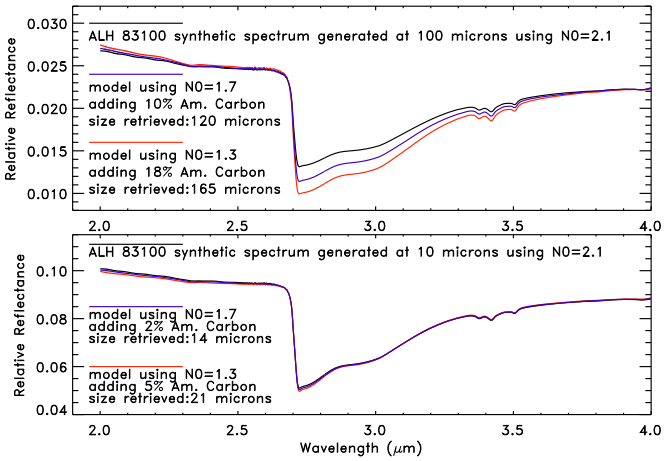

Fig. 1. Comparison of different synthetic spectra of the ALH 83100 sample generated using the Hapke model and optical constants retrieved with different initial n_0 parameters.

(Zubko et al. 1996), used as a dark and featureless constituent in the subsequent mixtures. The presence of amorphous carbon could physically and numerically accommodate small spectral differences. The new synthetic spectra were then generated considering optical constants generated at lower n_0 values (at 1.7 and 1.3). For this particular test, the free parameters in the models are the amount and size of each constituent in the mixture. In order to mimic the expected effects on the whole spectral range of the Bennu spectrum, we adjusted the synthetic spectra and computed the χ^2 using the errors estimated from the average spectrum of Bennu. The results are plotted in Fig. 1. The fits are very satisfactory with the particle size initialized at 10 μm. Indeed, the differences between the synthetic spectra are very small (i.e., it is possible to reproduce the entire shape of the initial spectrum) and the physical and chemical properties of the initial sample are well represented (i.e., the particle size is similar and the need for an additional featureless constituent is limited to a few percent). Problems arise at 100 μm, especially when the n_0 value is too far from the initial one (1.3 instead of 2.1), but the fits stay acceptable when the n_0 value differs by no more than 20% (1.7 instead of 2.1). In this last case, the particle size increases from 100 to 122 μm and the need for an additional featureless constituent reaches no more than 10%. Our conclusion at this step is that we should be careful in interpreting the model results in terms of the accuracy of the retrieved particle sizes and abundances. However, these optical constants are accurate enough to produce realistic synthetic spectra and provide a valuable tool to constrain the chemical and physical properties of the surface of Bennu.

4. Results

The first step of our analysis is to rank the different meteorite analogs (Table 1) using a direct comparison with the average reflectance spectrum of Bennu. For this purpose, we generated a simple intimate mixture of amorphous carbon with only one meteorite sample and for all available temperatures. Amorphous carbon is present in a wide range of meteorites (Murae et al. 1993), and it has been chosen as a dark and featureless end member. Table 2 reports the best 20 analogs in terms of reduced χ^2. The synthetic spectra of three of the best fits are presented in Fig. 2.

Table 2. Best 20 results, ranked by reduced χ^2 value, considering an intimate mixture of amorphous carbon with only one other analog from Table 1.

Rank	Analog	Temperature	red.χ^2	Per.
1	ALH 83100 *CM1/2*	150°C	5.95	80%
2	Essebi *C2-ung*	22°C	6.79	93%
3	Boriskino *CM2*	22°C	7.86	95%
4	Orgueil *CI1*	102°C(*)	8.11	92%
5	DOM 08003 *CM2*	150°C	9.38	46%
6	GRO 95577 *CR1*	150°C	9.43	32%
7	ALH 84044 *CM2*	150°C	10.24	32%
8	ALH 84044 *CM2*	22°C	11.62	8%
9	LON 94101 *CM2*	150°C	12.32	29%
10	DOM 08003 *CM2*	22°C	12.84	18%
11	LEW 85311 *CM2-an*	150°C	12.39	59%
12	Mokoia *CV3*	102°C(*)	12.97	99%
13	QUE 99355 *CM2*	22°C	13.78	7%
14	Nogoya *CM2*	22°C	13.81	13%
15	LEW 87022 *CM2*	22°C	14.49	56%
16	Niger *CM2*	22°C	15.47	19%
17	LON 94101 *CM2*	22°C	15.68	10%
18	MIL 07700 *CM2*	22°C	15.97	29%
19	Vigarano *CV3*	22°C	15.98	27%
20	QUE 97990 *CM2*	22°C	16.14	34%

Notes. The percentage (Per.) of the mixture accounted for by the other analog in each case is reported in the rightmost column. (*)Sample temperature reached ~102°C, but spectrum was taken after the sample had cooled.

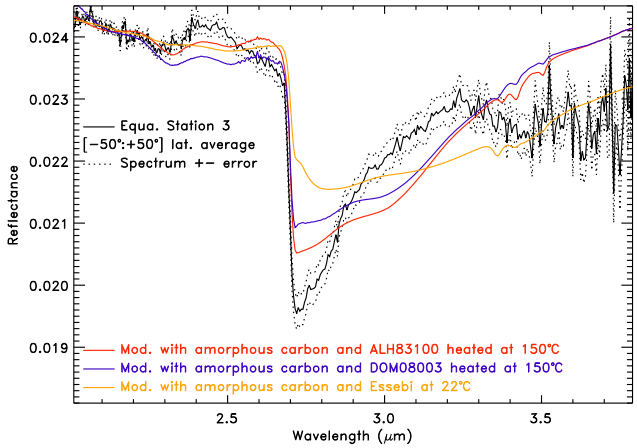

Fig. 2. Synthetic spectra obtained using an intimate mixture of amorphous carbon with ALH 83100, DOM 08003 (both heated at 150°C) or Essebi (obtained at 22°C), and the average spectrum of Bennu obtained during Equatorial Station 3 (±50°latitudinal range).

None of the materials considered in this work exhibit precisely the same spectral properties as those reported for Bennu in the [2–3.8] μm range. In general, the slope in the [2–2.65] μm range could be fitted with only one analog intimately mixed with amorphous carbon, but the broad 2.7 μm absorption band and the wavelengths longward of 3.3 μm are more difficult to reproduce using a simple model. The best results, in terms of the lowest reduced χ^2, are achieved mostly using CM chondrites (usually heated in laboratory), such as ALH 83100, Boriskono, DOM 08003, or ALH 84044. There are a few other chondrites having low reduced χ^2 values, such as Essebi (C2-ung), Orgueil (CI), or GRO 95577 (CR1) chondrites. Heating processes mainly affect the amount of adsorbed water of the samples and usually change the intensity and shape of the 3 μm band. At this step, we confirm that Bennu is spectrally most similar to CM meteorites and this strengthens previous speculations that Bennu may not fall into an existing carbonaceous chondrite group (see Hamilton et al. 2019; Kaplan et al. 2020, for instance). We then pursued the idea that a combination of several materials could fit the spectral properties of Bennu and give new insights as to the composition and physical properties of the surface of Bennu.

The number of different materials used in this work is large, so we did not attempt to produce all possible combinations. To obtain results that take into account a substantial but reasonable number of possible choices, we ran 1000 different spectral models. Each synthetic spectrum was computed assuming an intimate mixture of amorphous carbon, with four of the potential meteorite analogs listed in Table 1 chosen randomly. We limited the total number of different materials in a mixture to five because it appears that fits are usually achieved with rarely more than three or four different materials. Again, this choice helped to minimize the computation time. The free parameters are the particle sizes, the ratio of the different materials in the intimate mixtures, and the global photometric parameter (PHO), which accounts for $(1 + B(g))P(g) - 1$, as presented previously. We focused our analyses more particularly on the retrieved abundances and particle sizes, as constrained by the different models.

The results from these 1000 simulations show an improvement of the fits compared to those obtained considering only one CC mixed with amorphous carbon; the reduced χ^2 is divided by a factor of 2 at least, but it is always limited to ~2.8 at best (Fig. 3). We checked that all the individual samples presented in Table 1 have been used at least several times. This cannot fully ensure that we obtained the best achievable combination from our data set, but it allowed us to provide the main trends. In order to better rank the different materials, we computed what we call the fitting score (FS) of each constituent in each model. For each model, we computed FS for each constituent as the reduced χ^2 of the fit divided by the proportion of the constituent considered in the mixture. The advantage of FS is to consider the contribution (small or large) of each component, avoiding using the same value for all the components of a given mixture, as done in the previous analysis. Figure 3 presents this value for a restricted sample of constituents (each mixture gives a particular reduced χ^2). By extension, for a given material, we could also search for the minimal value (mFS) from all computed FS.

Good combinations for approximating the surface of Bennu appear in the left part of Fig. 3; the best analogs are concentrated in the upper left part of this figure, because a large amount of the materials is also required. These tend to be materials with low FS, such as Tagish Lake, LEW 87022, ALH 83100, and MCY 05230. These new models mainly confirm trends obtained in the previous section when considering a simple mixture of amorphous carbon with one other constituent, preferentially classified in the CM group. However, the results obtained with the association of several materials seem to indicate that C2-ungrouped meteorites, such as the sample of Tagish Lake published in Takir et al. (2019), could also be good analogs. Among the best analogs, as classified using mFS < 7.0 (a part of the list appears in the lower part of Fig. 3), we find thirteen chondrites from the CM group, three from the C2-ung group (Tagish Lake, Essebi, Bells), two from the CI group (Alais, Orgueil), one from the CR group (GRO 95577), and one from the CV3 group (Vigarano). These findings are compatible with those of Hamilton et al. (2020) and Kaplan et al. (2020) to some extent.

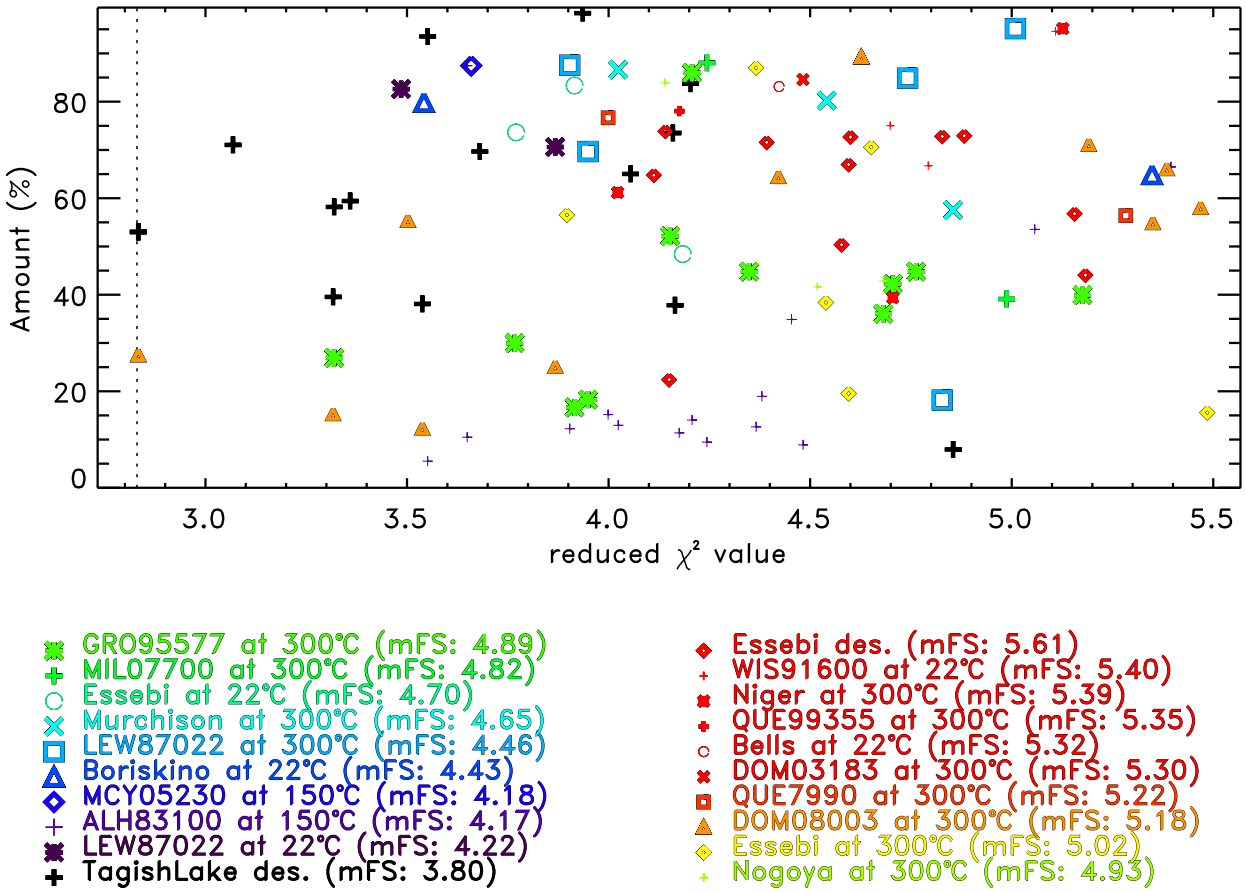

Fig. 3. Results showing only a part, for clarity, of the best fits obtained from our simulations (reduced $\chi^2 < 5.6$). For each reduced χ^2, the amount of each material, with low mFS in the models, is indicated. For example, there is a model (presented in Fig. 4) with a reduced χ^2 of ~2.83 (represented by the vertical dashed line) composed of ~53% of Tagish Lake (desiccated at 102°C), and ~27% of DOM 08003 (measured at 300°C). The remaining ~20% is Mokoia (measured at 300°C and not represented for clarity and due to its higher mFS). All constituents located in the upper left part represent the best analogs tested in this work for Bennu's surface. The legend below the plot reports the lowest 20 minimum FS (mFS) values obtained from our simulations.

The former find, from a more restricted set of analogs, that the CMs AhS91A_1 and ALH 83100, as well as the CI1 Orgueil, are the best analogs to reproduce the [7–30] μm range of Bennu spectra. They conclude that the bulk mineralogy of the sample returned to Earth from Bennu likely will be dominated by Mg-phyllosilicates, with some magnetite and a volume less than ~10% anhydrous silicates. The latter find minerals that are in the highly aqueously altered CM- and CI-group carbonaceous chondrites.

The presence of the CR chondrite GRO 95577 could appear incompatible, at first sight, with the main picture provided by this work, assuming that the surface of Bennu is mainly covered by materials having experienced similar histories of aqueous alteration and a thermal event. However, Beck et al. (2014) summarize that GRO 95577 was initially classified as a C2 chondrite and it was classified as a CR from its petrology and oxygen isotopic composition. From its IR spectrum alone, it is not possible to distinguish GRO 95577 from a heavily altered CM or CI. In addition to that, GRO 95577 phyllosilicates, as observed in the infrared, resemble saponite, possibly because of their poor crystallinity, as also observed for CMs.

We present two of the best models obtained from our simulation in Fig. 4. The first one was generated from a mixture of Tagish Lake, Mokoia, and DOM 08003, while the second model was generated from a mixture of Tagish Lake, Niger, and

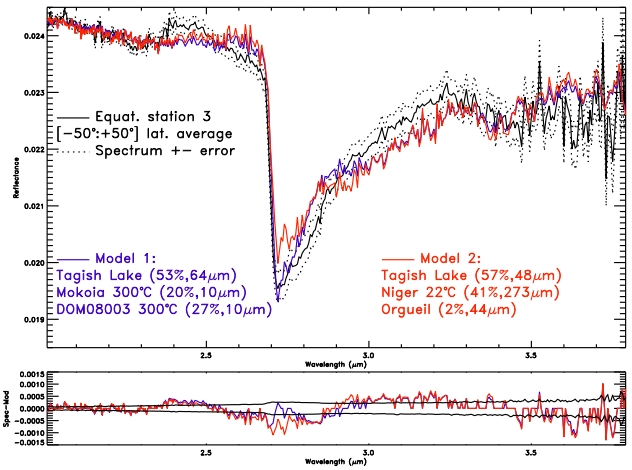

Fig. 4. *Top*: sample of two fits of Bennu (in color), for which the reduced χ^2 ~ 2.8–3.5. The synthetic spectra were generated using an intimate mixtures of small particles of Tagish Lake (desiccated at 102°C) mixed with other small constituents such as DOM 08003 and Mokoia (model 1), or mixed with larger particles of Niger (at 22°C) (model 2). The average spectrum of Bennu is shown by the solid black line, and errors appear as dotted black lines. *Bottom*: representation of Bennu spectrum minus the synthetic spectra (in color), compared with the computed error of the Bennu spectrum (in black).

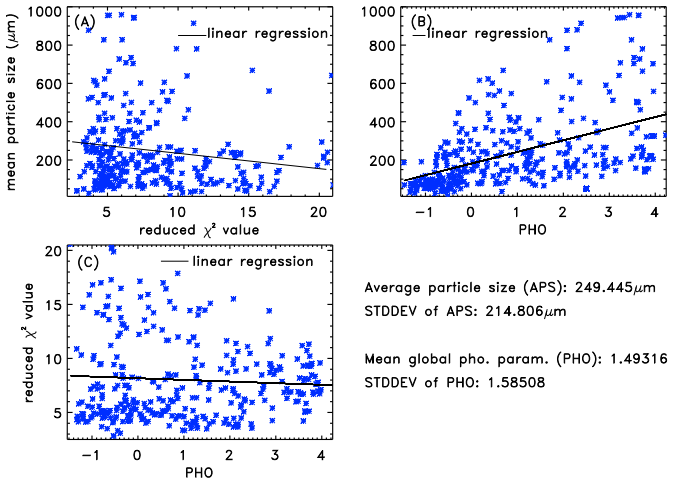

Fig. 5. *A*: mean particle size retrieved for each model as a function of the reduced χ^2. *B*: reduced χ^2 of each model as a function of the retrieved global photometric parameter (PHO). *C*: mean particle size retrieved for each model as a function of the retrieved PHO. The average particle size and the mean PHO, as well as their standard deviation, have been computed from all the models.

Orgueil. These models suggest the presence of small particles on Bennu, roughly in the [10–300] μm range. In order to check these values, we computed the average particle size from all our models. The average particle size for a given mixture was computed as the sum of the individual particle sizes multiplied by the proportion of the constituent considered in the mixture. We then computed the weighted average from all our models, taking the reduced χ^2 of each model into account as weight.

From this investigation, the average particle size was estimated at 250 ± 215 μm (the error represents one standard deviation). The average particle size seems to be slightly dependent on the quality of the fit, defined by the χ^2 value (see panel A from Fig. 5). From the linear regression, we could assume an average particle size to be a bit larger considering the better fits (i.e., up to 300 μm). Furthermore, a correlation exists between the average particle size and PHO (see panel B from Fig. 5), with larger particle sizes retrieved for higher PHO. The reduced χ^2 distribution versus PHO (see panel C from Fig. 5) indicates that the [−1:+4] range is favored and could produce models with similar reduced χ^2 (there is no apparent trend from the linear regression). From our simulations, we computed a mean PHO value ∼1.5 ± 1.6 (the error represents one standard deviation). Beyond this range, although the PHO value is not limited in our models, the number of cases drops. This could tentatively rule out lower and higher values, but our investigation is limited in constraining this parameter. Indeed, similar results could be achieved, at some points, tuning all the parameters of the model (i.e., size, abundance, and PHO). The highest PHO values retrieved from our models are compatible with values we can extract from photometric investigation in the literature (from Takir et al. 2015, for instance). Even if small particles, on the order of tens of microns, are still needed in our models, the literature gives a stronger case for an average particle size in the upper estimates (i.e., ∼300–350 μm). Considering that the surface of Bennu is dominated by boulders with little apparent fine-grained regolith (Lauretta et al. 2019; DellaGiustina et al. 2019), these small particle sizes suggest a coating of fine particulates on top of the boulder surface, supporting other findings from OSIRIS-REx data: Independent analyses of OTES observations (Hamilton et al. 2020) suggest that the spectral differences observed over Bennu's global surface could be attributable to the presence of a thin layer of fine particulates (<65–100 μm). The sizes retrieved by their models are consistent with thermal inertia results that limit any dust coating on Bennu's boulder-covered surface to <50 μm (Rozitis et al. 2020a).

At the detailed level, our models fail to fully and accurately reproduce the spectrum of Bennu within the error, in the spectral range covered in this paper (see bottom panel of Fig. 4). Nevertheless, though fits are not perfect and do not converge into a unique solution, our results dramatically reduce the number of possible analogs from the initial data set with which we started. As noted previously, the retrieved particle sizes must be treated with caution, but even with a conservative error (less than a factor of 2), the data indicate the presence of particles of tens to hundreds of microns in size.

To investigate the possible effects of the initial assumption of n and the global photometric value of $(1 + B(g))P(g) - 1$, we ran different spectral models using alternative optical constants. For this purpose, we fit the spectrum of Bennu by using the best intimate mixture found in our analysis considering Tagish Lake, Mokoia, and DOM 08003. We modeled five different sets of optical constants for Tagish Lake (summarized in Table 3), considering various initial n and $(1 + B(g))P(g) - 1$ values to extract k.

We find that the initial assumption of n does not significantly change the results when values are modified from 1.5 to 1.9. This outcome is consistent with what we previously presented when generating optical constants of ALH 83100 from absorbance spectra and considering various n_0 parameters. However, the abundances and particle sizes of the materials are more susceptible to change when changing the initial $(1 + B(g))P(g) - 1$ value. In our models, initialized values of ∼1 reduce the amount and particle size of Tagish Lake and amorphous carbon constituents and increase the amount of finer Mokoia and DOM 08003 particles. When this parameter is set at approximately −1, the amount and particle size of Tagish Lake material increase.

These results confirm that the modeled values provided from the abundances and particle size should be used with caution, given that the initial parameters are not yet well constrained. In addition, the five models considered in this subsection yield similar reduced χ^2 (within 7%) and we cannot discard any of the solutions within this criterion. However, we can confidently report from the different optical constants used in these five models that the abundance of Tagish Lake-like material in the best mixture is close to 50%, and particles are mainly on the order of tens of microns.

5. Discussion

The results obtained in this work are based on spectral modeling, restricted by a large but ultimately limited number of samples. Beyond the fact that we probably do not have the ultimate candidate to reproduce the entire spectrum of Bennu exactly, and that the optical constants extracted in this work could be improved, we could also infer limits of our models due to the restricted set of temperatures investigated in laboratory for each sample. As presented in Beck et al. (2014) or Takir et al. (2019), temperatures reached for each sample greatly modify the bulk composition, and then modify the spectral behavior. The main spectral changes occur when removing variable amounts of adsorbed water when the temperature reaches but does not strongly exceed ∼100°C in a laboratory environment. At warmer temperatures, structural water bound into the mineral

Table 3. Results of spectral modeling considering different optical constants of Tagish Lake, generated using different initial n and $(1 + B(g))P(g) - 1$ values to extract k.

Pho. [(a)]	n [(a)]	Red. χ^2	*Pho.* [(b)]	Tagish Lake (%-μm)		Mokoia (%-μm)		DOM 08003 (%-μm)		Amor.Ca (%-μm)	
−0.9	1.5	3.03	−0.871	69	57	15	15	10	37	6	20
−0.9	1.9	3.05	−0.862	68.5	56	15	14	10	35	6.5	24
0.1	1.7	2.98	−0.773	50	39	27	7	16	11	7	10
0.9	1.5	2.84	−0.686	51.5	35	23	8	24.5	13	1	10
0.9	1.9	2.80	−0.752	42	44	31	5	27	8	–	–

Notes. For a given set of parameters set to generate the Tagish Lake optical constants, this table indicates the following: the reduced χ^2 of the fit, the $(1 + B(g))P(g) - 1$ value of the entire mixture as provided by the fit, and the amount and size of the materials considered for each case. [(a)]Initialized $(1 + B(g))P(g) - 1$ and n values to compute k of Tagish Lake. [(b)]$(1 + B(g))P(g) - 1$ provided by the fit.

structure could also be modified, with various effects in the reflectance spectrum in the [2.7–3.3] μm range. The content of carbonates and organic matter are also dependent on the heating level; this could affect the reflectance spectrum in the [3.3–3.6] μm range.

Our findings indicate that a mixture of C2-ung, CM, and possibly CI materials is the best analog for Bennu's surface. Global analyses do not support either strong latitudinal or longitudinal spectral variations and, as such, we can cautiously expect that this finding applies across the whole surface of Bennu, except in peculiar areas observed at a higher spatial resolution (Barucci et al. 2020). Beck et al. (2014) show a correlation between the classification of carbonaceous chondrites based on spectral parameters such as the 3 μm band intensity and the 11.2 μm band intensity in their absorbance data. These two criteria are very good proxies to retrieve the hydration state and olivine content of the chondrites, respectively, and provide information about the formation and evolution of Bennu. Unfortunately, from the best analogs suggested by our simulations, we cannot draw any clear conclusions about these components. Indeed, some of the best analogs present a high level of hydration and low olivine content (DOM 08003, ALH 83100), others present a moderate level of hydration and average content of olivine (Tagish Lake, Essebi, Niger), and marginal cases present a very low level of hydration and high olivine content (Vigarano). Based on the 3 μm band intensity reported from the reflectance spectrum, we can rule out null or low levels of hydration, but we cannot draw clear conclusion because we cannot accurately convert the reflectance value into units of absorbance (the unit used in Beck et al. 2014). In our simulations, most of the best results were mainly obtained with data from samples that were heated in the laboratory. This finding seems to be compatible with the ambient conditions on Bennu (Rozitis et al. 2020b). There are exceptions among the best analogs (with mFS < 7) that could hamper this trend: LEW 87022, Boriskono, and Essebi, which are preferentially used by the models when measured at room temperature (~22°C). Further detailed laboratory analyses, focused on the effect of the temperature (i.e., with more than three different temperatures) would provide more insight on this topic.

If confirmed, the fact that one small rubble pile asteroid has similarities with different kinds of chondrites, such as CMs, CIs, and marginally a few CVs, could be puzzling. These different carbonaceous chondrites do indeed have different isotopic ratios, hydration levels, and different carbon contents, implying accretion of the carbonaceous asteroids near the snow line, but at increasing heliocentric distances for increasing water/rock ratios (see Marrocchi et al. 2018, for instance). From multispectral images, DellaGiustina et al. (2020) attribute the reflectance and color variation to a combination of primordial heterogeneity and varying exposure ages. They conclude that boulders on Bennu may have originated from different zones within the parent body and that the multimodal distribution of the boulder populations implies that different processes, such as aqueous alteration and heating, led to their distinct spectrophotometric properties. This scenario could explain the results of our analysis. This also suggests that the parent body of Bennu was formed a little bit farther from the snow line to enable the CM and CI-like properties, at least in its interior. The presence of CV-like properties implies a transition or evolution of the parent body inward, closer to the Sun.

6. Conclusions

From simulations based on laboratory measurements of meteorites and 1000 synthetic spectra generated using the Hapke model, covering the [2.0–3.8] μm range, we find that the mean reflectance spectrum of Bennu is best fitted by an intimate mixture of several possible carbonaceous chondrite analogs, specifically the following.

1. A few members of the C2-ung, CM, and, to some extent, CI groups are the best possible analogs to reproduce the spectral behaviors of Bennu's surface, when mixed together. Even if there is not a unique solution, Tagish Lake seems to be one of the samples best able to reproduce the behavior of the reflectance spectrum of Bennu in the [2–3.8] μm range, when intimately mixed with CM components, such as DOM 08003 (heated at 300°C) or Niger (measured at 22°C).
2. The models suggest the presence of particles on the order of tens to a few hundreds of microns on the surface of Bennu. As Bennu's surface is visibly covered by boulders, this result suggests the presence of fine particulates on top of the surface elements of Bennu, consistent with previous findings.

We can consider these properties to be applicable to the whole surface of Bennu, given that a global spectral analysis, performed at the identical spatial resolution, by multivariate statistics indicates a relative homogeneous surface, except for a few peculiar areas observed at a higher spatial resolution (Barucci et al. 2020). From our investigation, Bennu does not seem to be similar to any known meteorite, but more similar to a mixture of various materials. This conclusion is consistent with those of other kinds of investigation (Hamilton et al. 2020; Kaplan et al. 2020). The sample that OSIRIS-REx will return in 2023 will reveal the composition of the Bennu's surface and the limitations of the method we used. The conclusions of this paper should be confirmed by additional models accounting for the

whole wavelength range covered by OVIRS, but new laboratory data are required for this purpose.

Acknowledgements. This material is based on work supported by NASA under Contract NNM10AA11C issued through the New Frontiers Program. F.M., M.A.B., P.H., A.P., J.D.P.D. and S.F. acknowledge funding support from CNES. We thank P. Beck for his helpful support in making use of the absorbance data and A. Raponi for his comments to improve the quality of this paper. We are grateful to the entire OSIRIS-REx Team for making the encounter with Bennu possible.

References

Ballouz, R.-L., Walsh, K. J., Barnouin, O. S., et al. 2020, Nature, 587, 205
Barucci, M. A., Hasselmann, P. H., Praet, A., et al. 2020, A&A, 637, L4
Beck, P., Garenne, A., Quirico, E., et al. 2014, Icarus, 229, 263
Binzel, R. P., DeMeo, F. E., Burt, B. J., et al. 2015, Icarus, 256, 22
Bottke, W. F., Moorhead, A. V., Connolly, H. C., et al. 2020, J. Geophys. Res. Planets, 125, e06282
Clark, B. E., Binzel, R. P., Howell, E. S., et al. 2011, Icarus, 216, 462
Christensen, P. R., Hamilton, V. E., Mehall, G. L., et al. 2018, Space Sci. Rev., 214, 87
Davidson, J., Krot, A. N., Nagashima, K., et al. 2014, Meteorit. Planet. Sc., 49, 1456
DellaGiustina, D. N., Emery, J. P., Golish, D. R., et al. 2019, Nat. Astron., 3, 341
DellaGiustina, D. N., Burke, K. N., Walsh, K. J., et al. 2020, Science, 370, eabc3660
Emery, J. P., & Brown, R. H., 2004, Icarus 170, 131
Fornasier, S., Hasselmann, P. H., Deshapriya, J. D. P., et al. 2020, A&A, 644, A142
Golish, D. R., Shultz, N. K., Becker, K. J., et al. 2021, Icarus, 355, 114133
Hamilton, V. E., Simon, A. A., Christensen, P. R., et al. 2019, Nat. Astron., 3, 332
Hamilton, V. E., Kaplan, H. H., Christensen, P. R., et al. 2020 A&A, submitted
Hapke, B., 1981, J. Geophys. Res., 86, 4571
Hapke, B., 1984, Icarus, 59, 41
Hapke, B., 1986, Icarus, 67, 264
Hapke, B., 1993, Topics in Remote Sensing (Cambridge, UK: Cambridge University Press)
Hapke, B., 2008, Icarus, 195, 918
Kaplan, H. H., Lauretta, D. S., Simon, A. A., et al., 2020, Science, 370, eabc3557
Kitazato, K., Milliken, R. E., Iwata, T., et al. 2019, Science, 364, 272
Lauretta, D. S., Balram-Knutson, S. S., Beshore, E., et al. 2017, Space Sci. Rev., 212, 925
Lauretta, D. S., Dellagiustina, D. N., Bennett, C. A., et al. 2019, Nature, 568, 55
Lauretta, D. S., Enos, H. L., Polit, A. T., Roper, H. L., & Wolner, C. W. V. 2021, in Sample Return Missions, ed. Longobardo, A. (Amsterdam: Elsevier), ch. 8
Levenberg, K. 1944, Quart. Appl. Math., 2, 164
Marquardt, W. 1963, J. Soc. Indus. Appl. Math., 11, 431
Marrocchi, Y., Bekaert, D., & Piani L. 2018, Earth Planet. Sci. Lett., 482, 23
Molaro, J. L., Walsh, K. J., Jawin, E. R., et al. 2020, Nat Commun., 11, 2913
Murae, T., Kagi, H., & Masuda, A. 1993, Primitive Solar Nebula and Origin of Planets (Tokyo: Terra Scientific Publishing Company), 479
Reddy, V., Dunn, T. L., Thomas, C. A., et al. 2015, Asteroids IV (Tucson: University of Arizona Press), 43
Reuter, D. C., Simon, A. A., Hair, J., et al. 2018, Space Sci. Rev., 214, 54
Reuter, D. C., Simon, A. A., Lunsford, A., et al. 2019, NASA Planetary Data System (USA: NASA)
Rocha, W., R., M., & Pilling, S. 2014, Mol. Biomol. Spectr., 123, 436
Roush, T. L. 2003, Meteorit. Planet. Sci., 38, 419
Rozitis, B., Ryan, A., Emery, J., et al. 2020a, Sci. Adv., 6, eabc3699
Rozitis, B., Emery, J. P., Siegler, M. A., et al. 2020b, J. Geophys. Res. Planets, 125, e06323
Simon, A. A., Reuter, D., Gorius, N., et al. 2018, Remote Sens., 10, 1486
Simon, A. A., Kaplan, H. H., Hamilton, V. E., et al. 2020, Science, 370, eabc3522
Takir, D., Clark, B. E., Drouet d'Aubigny, C., et al. 2015, Icarus, 252, 393
Takir, D., Stockstill-Cahill, K. R., Hibbitts, C. A., et al. 2019, Icarus, 333, 243
Yang, B., & Jewitt, D. 2010, AJ, 140, 692
Zou, X.-D., Li, J.-Y., Clark, B. E., et al. 2020, Icarus, 358 114183
Zubko, V. G., Mennella, V., Colangeli, L., & Bussoletti, E. 1996, Formation of Stars (Hoboken: wiley), 333